



**HAL**  
open science

## High-Fidelity Computational Analysis of an Energy-Saving Device at Model Scale

Michel Visonneau, Ganbo Deng, Patrick Queutey, Emmanuel Guilmineau,  
Alvaro del Toro Llorens

► **To cite this version:**

Michel Visonneau, Ganbo Deng, Patrick Queutey, Emmanuel Guilmineau, Alvaro del Toro Llorens. High-Fidelity Computational Analysis of an Energy-Saving Device at Model Scale. Hull Performance & Insight Conference (HullPIC), Apr 2016, Turin, Italy. hal-02566713

**HAL Id: hal-02566713**

**<https://hal.science/hal-02566713>**

Submitted on 7 May 2020

**HAL** is a multi-disciplinary open access archive for the deposit and dissemination of scientific research documents, whether they are published or not. The documents may come from teaching and research institutions in France or abroad, or from public or private research centers.

L'archive ouverte pluridisciplinaire **HAL**, est destinée au dépôt et à la diffusion de documents scientifiques de niveau recherche, publiés ou non, émanant des établissements d'enseignement et de recherche français ou étrangers, des laboratoires publics ou privés.

# High-Fidelity Computational Analysis of an Energy-Saving Device at Model Scale

Michel Visonneau, ECN, LHEEA, Nantes/France, [michel.visonneau@ec-nantes.fr](mailto:michel.visonneau@ec-nantes.fr)

Ganbo Deng, ECN, LHEEA, Nantes/France, [ganbo.deng@ec-nantes.fr](mailto:ganbo.deng@ec-nantes.fr)

Patrick Queutey, ECN, LHEEA, Nantes/France, [patrick.queutey@ec-nantes.fr](mailto:patrick.queutey@ec-nantes.fr)

Emmanuel Guilmineau, ECN, LHEEA, Nantes/France, [emmanuel.guilmineau@ec-nantes.fr](mailto:emmanuel.guilmineau@ec-nantes.fr)

Alvaro del Toro Llorens, NUMECA Int., Brussels/Belgium, [alvaro.deltorollorens@numeca.be](mailto:alvaro.deltorollorens@numeca.be)

## Abstract

*This paper presents a thorough computational study of the flow around the Japan Bulk Carrier (JBC) with or without an Energy Saving Device (ESD) in front of the propeller. This study conducted at model scale was performed in the framework of the Tokyo 2015 Workshop on Numerical Ship Hydrodynamics. Configurations with and without ESD, with and without propeller are compared and analysed and conclusions about the efficiency of this specific ESD at model scale are drawn.*

## 1. Introduction

The Japan Bulk Carrier (JBC) is a Capesize bulk carrier equipped with a stern duct as an energy saving device (ESD). National Maritime Research Institute (NMRI), Yokohama National University and Ship Building Research Center of Japan (SRC) were jointly involved in the design of this ship hull, duct and rudder. Its length between perpendiculars is  $L_{pp}=280\text{m}$ . Its service speed is 14.5 knots, leading to a Froude number  $Fn=0.142$  and a Reynolds number at model scale of  $Re=7.46\cdot 10^6$ . Towing tank experiments were performed at NMRI, SRC and Osaka University, including resistance tests, self-propulsion tests and PIV measurements of stern flow fields. Several test cases were considered, all with free sinkage and trim; test cases 1.3a (resp. 1.4) are for towing test without (resp. with) ESD, cases 1.7 (resp. 1.8) for self-propulsion tests without (resp. with) ESD. Global force measurements and local LDV velocity profiles at three sections named S2, S4 and S7 before and after the propeller and duct were also provided by the organizers. Figs. 1 and 2 show a view of the stern without and with ESD with the location of the local measurement sections.

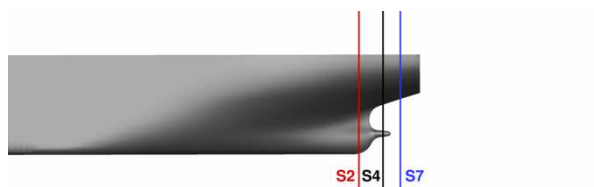


Fig.1: Side view of the hull without ESD

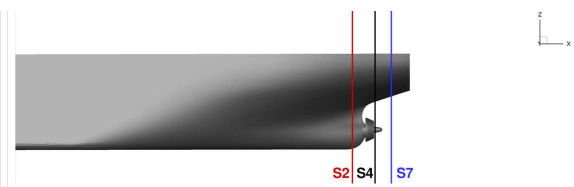


Fig.2: Side view of the hull with ESD

This paper presents a computational study of the flow around this ship with or without these specific appendages in order to analyze the physics of this complex flow configuration. Comparison with available experimental results will be shown. Also a careful verification exercise will be provided to get access to an evaluation of the discretization error.

It is well accepted now that CFD (Computational Fluid Dynamics) is a mature tool for steady-state ship hydrodynamic applications such as resistance in calm water. Accurate enough predictions can be obtained with reasonable resources even for fully appended hulls, both for model and full scale in a routine design procedure. However, rigorous V&V (verification & validation) exercises are seldom performed by CFD users. In most of the cases, one grid and one computation are adopted following guidelines based on recommendations and experience. The recommended setup (such as grid density, turbulence model, etc.) may differ from one institution to another. Comparison with measurement data is often the only criterion when establishing those guidelines. The versatility of a guideline thus

established can be questionable, since a small comparison error can be the result of error cancellation between numerical discretization and physical modeling errors. By performing a careful V&V exercise, one attempts to quantify turbulence modeling error and tries to answer questions such as whether a non-linear turbulence model is more accurate than a linear turbulence model for ship resistance prediction, what is the impact on the accuracy when a wall function is used, etc.

Compared with resistance computations, validation for propulsion computations is much more challenging. To our knowledge, the only approach capable of accurately predicting ship propulsion power is to simulate directly the rotating propeller with sliding grid or overset approaches. Time-accurate simulation with very small time steps is required for such simulation even if time-averaged solution is sufficient. Our experience with V&V exercises show that reliable numerical uncertainty estimations are nearly impossible for this case due to the high iterative error as well as the time discretization error. Self-propulsion simulations may also model the effect of the propeller by body forces in the RANSE solver. With such an approach, propeller thrust can be provided by the RANSE solver. But to determine propeller revolution rate and propeller torque, a simplified model or a coupling approach between RANSE solver and another specific solver simulating the propeller such as RANSE/BEM coupling approach must be used.

## 2. Numerical approach and case setup

Computations were performed with the ISIS-CFD flow solver developed by our team, also available in the commercial software FINE<sup>TM</sup>/Marine. It is an unstructured finite volume RANSE solver using a free-surface capturing approach. For technical details of the solver, we refer to *Queutey and Visonneau (2007)* and *Wackers et al. (2012)*.

Except for the case when propeller motion is resolved by the RANSE solver, only a half domain is simulated. The inlet boundary is located at  $2.5L_{pp}$  from FP (forward perpendicular), the outlet at  $3.0L_{pp}$  after AP (aft perpendicular). Bottom and top boundaries are located at  $1.5L_{pp}$  and  $0.5L_{pp}$  from the waterline, respectively. The lateral boundary is located at  $1.5L_{pp}$  from the mid plane. A pressure boundary condition is applied at the bottom and top boundaries, while a far-field boundary condition is applied at the inlet, outlet, as well as the lateral boundary. One relies on the Richardson extrapolation for the V&V exercise. The Richardson extrapolation can be applied only when grid similarity is ensured while the unstructured hexahedral mesh generator Hexpress<sup>TM</sup> available in FINE<sup>TM</sup>/Marine is employed in the present study. With Hexpress<sup>TM</sup>, it is hardly possible to generate a set of rigorously similar grids. But with a special setup, it is possible to ensure grid similarity before the insertion of viscous layer. Our experience shows that grids thus generated usually allow a successful Richardson extrapolation. This grid generation setup is too specific to the grid generator Hexpress<sup>TM</sup> and will not be described here. We refer interested readers to *del Toro (2015)* for details. Table 1 gives the number of grid cells for the different grid sets used here.

Table 1: Number of grid cells for different cases

Cases	Grid 4	Grid 3	Grid 2	Grid 1
1.1a_wm	405K	1.512M	3.143M	5.724M
1.1a_wr	861K	2.632M	5.304M	9.197M
1.2a_wm	725K	2.311M	4.806M	8.750M
1.2a_wr	1.317M	4.269M	8.344M	14.077M
1.5a_wm	2.442M	4.784M	10.247M	18.676M
1.6a_wm	2.513M	6.668M	13.913M	25.332M

In Table 1, case 1.1a (resp.1.2a) stands for the naked hull (resp. hull with ESD) while case 1.5a (resp. 1.6a) stands for hull with propeller (resp. hull with propeller and ESD). "wm" stands for wall modelled simulation for which wall function approach is used, "wr" for wall resolved simulation for which a near wall low-Reynolds turbulence model is employed. For the first case, the same  $y^+$  value of about 30 is applied for all grids, while for the second case, the  $y^+$  value changes from about 0.4 for

the coarsest grid to about 0.16 for the finest grid. Meshes for different configurations have similar grid density. The difference in number of cells is due to the presence of the energy saving device (ESD) and the propeller, additional cells in the viscous layer when using wall resolved approach, and whole domain simulation rather than half domain simulation. Mesh density is not too fine. Mesh size near the free-surface is about  $0.0008L_{pp}$  for the fine mesh. Grids 1 and 2 represent meshes commonly used for resistance computation for engineering application. Unless otherwise stated, all computations were performed with the non-linear EASM turbulence model. A second-order upwind blended scheme was employed for spatial discretization except for the case with propeller resolved simulation for which a more stable ALVSMART scheme is used.

## 4. Results and discussions

### 4.1 Resistance Results for the JBC test cases

Tables 2 and 3 give main results for total resistance for case 1.1a (without ESD) and 1.2a (with ESD) respectively. We give only the finest grid solution U1, the observed order of convergence  $p$ , Richardson extrapolation error RE% defined as  $(\delta_{RE}-U1)/\delta_{RE} \times 100$ , and the comparison error E%D defined as  $(D-S)/D \times 100$  where  $D$  is the measurement data.  $S=U1$  is the simulation result.  $\delta_{RE}$  is the result of Richardson extrapolation. The least squared approach proposed by *Hoekstra and Eca (2008)* is used for Richardson extrapolation. When the observed order of convergence is higher than 2.1, Richardson extrapolation is obtained with assumed second-order accuracy. For both cases, the EASM model gives better prediction than the SST model. Moreover, the numerical discretization error is smaller than the difference due to turbulence model for the fine grid. Hence, when the grid is fine enough, the EASM model should give better prediction for ship resistance for this test case. The reason for the better performance with the EASM model is due to the existence of a relatively strong aft-body vortex for this geometry. When the aft-body vortex is not so strong, the SST model should also be capable to give an accurate prediction for ship resistance as well. Even with a fine grid containing more than 6M cells, numerical discretization error for resistance computation is still about 2% at least. Hence, when the grid is further refined, the EASM model is expected to under-estimate the resistance by about 4% for the case without ESD, and 3% for the case with ESD. This is confirmed by computations with adaptive grid refinement which give a comparison error of 3.1% for the case without ESD, and 2.2% for the case with ESD. For both cases, the use of wall function does not deteriorate too much the predicted result. The predicted resistance differs only by 0.1% and 0.45% respectively, which is much smaller than the discretization error. This observation justifies the use of a wall function for engineering applications due to much lower computation cost. Flow separation is observed on the ESD, Fig. 4. This might explain why the comparison error, the Richardson extrapolation error, and the observed order of convergence are higher for the case 1.4 when the wall function is used.

Table 2: Total resistance for case without duct and propeller (case 1.1a)

Simulation	U1	p	RE%	E%D
easm_wm	4.209	2.07	-2.3	1.87
easm_wr	4.213	1.94	-2.0	1.77
sst_wr	4.087	1.59	-3.2	4.71

Predicting pressure resistance with good accuracy is a challenging task for CFD. Fig. 3 shows the Richardson extrapolation error for pressure resistance for the case without ESD. Even with the finest grid, the error is still about 10% for the EASM model.

Table 3: Total resistance for case with duct but without propeller (case 1.2a)

Simulation	U1	p	RE%	E%D
easm_wm	4.200	2.93	-4.3	1.48
easm_wr	4.219	2.06	-2.3	1.03
sst_wr	4.093	1.67	-3.2	3.99

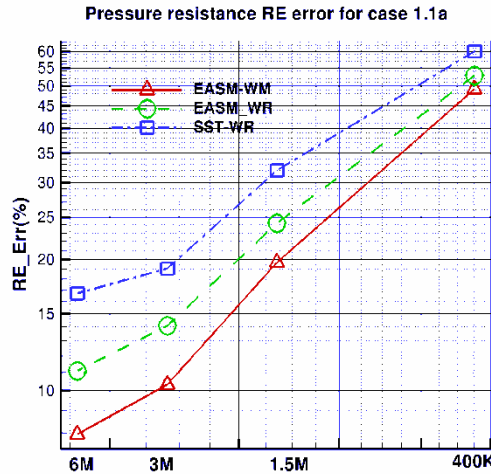


Fig.3: Richardson extrapolation error for pressure resistance

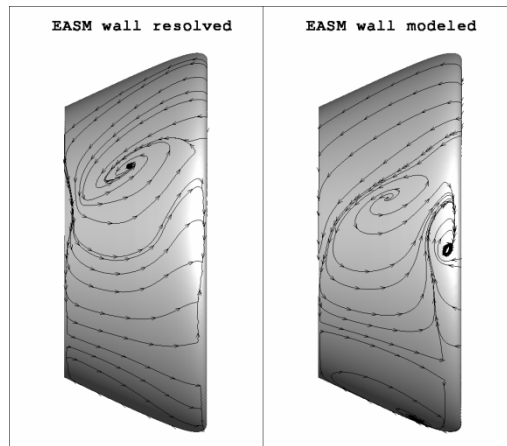


Fig.4 : Local view of the recirculation region on the duct with the EASM turbulence closure without or with wall function

Much higher uncertainty is observed for the SST model. But such high level of numerical uncertainty might be due to observed low order of convergence (1.53). As pressure resistance represents only about 25% of the total resistance, the numerical error observed in total resistance comes mostly from pressure resistance error. For applications where the contribution of pressure resistance becomes more important, e.g. vessels with smaller L/B ratio, higher grid resolution might be needed to achieve acceptable accuracy.

#### 4.2 Self-Propulsion Results for JBC test cases

The most obvious approach to perform a self-propulsion computation is to simulate the rotating propeller with the RANSE solver using sliding grid or overset grid approaches. A sliding grid approach is employed in our computations. With such an approach, time-accurate simulation is required even when only time-averaged results are needed. A rigorous V&V study with such a procedure requires numerical uncertainty estimation on space and time. Due to high computational cost, we did not attempt to assess the time discretization error. Instead, the time step and the non-linear iteration number per time step were chosen according to open-water computations using the same grid for the propeller. A sliding grid approach gives almost the same result for the propeller thrust compared with a computation performed in rotating frame. This "calibration" yields 150 time steps per revolution and 15 non-linear iterations per time step. One performs a first computation with a large time step to accelerate the ship to target speed until convergence. The rotating-frame approach is applied to the propeller domain. Ship trim and sinkage are computed during this computation. Then, in a restart

computation, one switches to a small time step (150 time steps per revolution). Ship motion is frozen during this computation and therefore, during this restart, ship dynamic position is not computed accurately. In our propeller-resolved simulation, computations were performed with the EASM model using wall function only. Computations were performed on 4 grids with different grid density as the cases for resistance computation. Figs. 5 and 6 show the evolution of force imbalance in our simulation for case 1.5a and 1.6a, respectively. 0.5N imbalance represents about 1.2% ship resistance. The force imbalance is expected to vanish under self-propulsion condition. The raw data are highly fluctuating due to rotating propeller. Results shown are smoothed by applying 1000 passes with the smoothing operation available in the Tecplot post-processor. The force imbalance obtained on the coarsest mesh is not shown. It was very high ( $\sim 8N$ ).

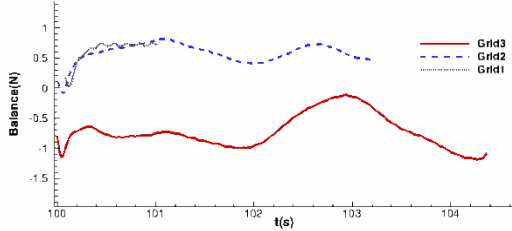


Fig.5: Force imbalance for case 1.5a (with propeller, without ESD)

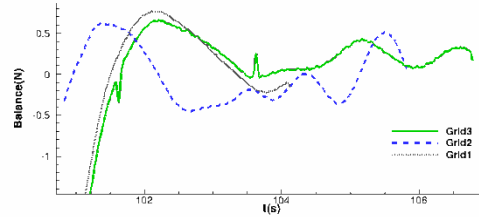


Fig.6: Force imbalance for case 1.6a (with propeller, with ESD)

Such high force imbalance is due to the very strong flow separation at the stern, resulting in a highly asymmetric wake. In our simulation, the propeller revolution rate was prescribed with the measurement value. Propeller thrust is positive. For the case without ESD, the force imbalance has a positive sign on the fine mesh (Grid1), i.e. propeller thrust is too high. We need to reduce propeller revolution rate to satisfy the self-propulsion condition. For the case with ESD, we are close to the self-propulsion condition. For case 1.6a, we performed about 7 seconds physical time, namely more than 50 propeller revolutions. With 150 time steps per revolution and 15 non-linear iterations per time step, the CPU cost is equivalent to about 30 resistance computations. Yet, it is hardly possible to determine a converged value for the force imbalance. Due to this convergence behaviour, we believe that the iterative error in our simulation is much higher than the discretization error. Hence, it is impossible to perform any reliable uncertainty estimation for a discretization error.

Table 4: Comparison error for propeller resolved simulation

	Case 1.5a		Case 1.6a	
	Value	E%D	Value	E%D
Ct*1000	4.661	3.11	4.572	3.99
Kt	0.214	1.47	0.227	2.78
Kq	0.029	-5.55	0.031	-3.52

Table 4 presents the predicted results with the finest grid for Ct, Kt and Kq as well as relative errors compared with measurement data. In spite of the high numerical uncertainty, the predicted results are reasonable. High propeller torque is a typical result for RANSE simulation when turbulence transition is not simulated. But as shown in the following section, the accuracy of the wake flow prediction can be the cause of such an over-prediction as well. It should be stressed that propeller thrust and ship resistance are not clearly defined in a propeller-resolved RANSE simulation. They are evaluated during post-processing using a procedure that is not always clearly defined. Concerning our results, we consider the dynamic axial force acting on the propeller domain as propeller thrust. This choice is justified by the fact that propeller thrust thus obtained agrees with the simulation using actuator disk approach presented later in this paper. With this post-processing procedure, we underestimate propeller thrust and ship resistance compared with measurement data. If we consider axial force acting on propeller blades as propeller thrust, then for case 1.6a, we will overestimate propeller thrust

by 1.2% and underestimate ship resistance by 2%. This results in a better agreement with measurement data, while it is exactly the same simulation result.

We have also performed self-propulsion simulations by using a body-force approach with an actuator disk model. Propeller thrust can be determined directly from the RANSE computation. But to determine other quantities related to propeller performance, such as propeller torque and propeller revolution rate, a special coupling procedure is required. The RANSE solver can be coupled with a BEM code or another type of simplified code to simulate the action of the propeller. In the present study, we employed a simpler approach without using any other simplified code. We only used the open-water  $K_t$ - $K_q$  results obtained from the measurements to determine the missing quantities in post-processing. The procedure is as follows. First, we perform a usual RANSE computation with an actuator disk approach to simulate the effect of the propeller. Propeller thrust is adjusted during this computation such that a self-propulsion condition is satisfied. After having obtained the converged solution with the RANSE solver, we compute the total velocity at the propeller plane. The total velocity is computed on a disk with the same size as the propeller diameter. This gives us two conditions: propeller thrust and total velocity. We perform an additional open-water computation using an actuator disk approach based on the open-water  $K_t$ - $K_q$  result. In this open-water actuator disk computation, propeller revolution rate and propeller advancing speed are adjusted such that the propeller thrust determined from the  $K_t$ - $K_q$  result and the total velocity computed at the propeller plane are the same as the values obtained with the RANSE computation with the hull. With two conditions and two unknowns, the problem is well defined and can be solved iteratively. Compared with more complex coupling procedures such a RANSE/BEM coupling approach, there is no need to compute the propeller induced velocity.

Table 5: Propeller modeled simulation for case 1.5a

	Wall resolved		Wall modeled	
	Value	E%D	Value	E%D
$C_t*1000$	4.625	3.87	4.620	3.97
$K_t$	0.214	1.24	0.213	1.84
$K_q$	0.0291	-4.41	0.0291	-4.19
$n(\text{rps})$	7.60	2.56	7.62	2.31

Table 6: Propeller modeled simulation for case 1.6a

	Wall resolved		Wall modeled	
	Value	E%D	Value	E%D
$C_t*1000$	4.660	2.14	4.617	3.04
$K_t$	0.2385	-2.36	0.2327	0.13
$K_q$	0.0306	-3.66	0.0305	-3.25
$n(\text{rps})$	7.31	2.53	7.33	2.27

Unlike for resistance computations, it is hardly possible to obtain a result with a good convergence behavior with respect to the requirement for Richardson extrapolation. Therefore, only the predicted  $C_t$ ,  $K_t$ ,  $K_q$  and propeller revolution rate  $n$  obtained with the finest grid as well as the relative errors compared with measurement data are shown in Tables 5 and 6 for the cases without and with ESD, respectively, both for wall resolved simulation and for wall modeled simulation using wall function. Unlike for propeller-resolved simulations, propeller thrust and ship resistance are clearly defined in the propeller-modeled RANSE computation. Compared with measurement data, predicted results are slightly better than what we obtained with the much more expensive propeller-resolved simulation presented in Table 4. As the computations are performed with half domain, propeller tangential forces are not taken into account. Errors due to this approximation need to be investigated in a future study. In our simulation, the measured  $K_t$ - $K_q$  are employed to determine propeller torque coefficient  $K_q$  and propeller revolution rate  $n$ . Propeller torque is over-predicted in the propeller-resolved simulation. In spite of the uncertainty about the accuracy of such simplified approach, we believe that such overprediction of propeller thrust can be attributed to the accuracy of the predicted wake. As shown in

the following sub-section, the predicted axial velocity at propeller plane is smaller than the measurement result, especially for the case without ESD. This explains why the estimated propeller revolution rate is lower and the propeller torque higher. In both cases, wall-resolved simulations and wall-modeled simulations give about the same accuracy. This justifies once again the use of wall functions for engineering applications.

### 4.3 Local Flow Results for JBC

#### 4.3.1 Mesh influence on the flow around the naked hull without ESD or propeller

The mesh set employed in the present study is designed to ensure an accurate enough accuracy for ship resistance and propulsion prediction based on our experiences. Spatial resolution in the wake near the propeller plane is about  $0.00086L_{pp}$  with the finest grid. With such a grid resolution, the difference of the predicted axial velocity contours obtained with the two finest grids is still clearly visible as shown in Fig. 4. Thus a grid independent solution for the local flow field has not yet been reached. Therefore, we attempted to obtain a more accurate solution with adaptive grid refinement, first without taking into account the free-surface. Results obtained with a double model computation using wall resolved EASM are shown in Fig. 7. The adaptive mesh contains about 35M cells. Comparison with measurement data is shown in Fig. 8.

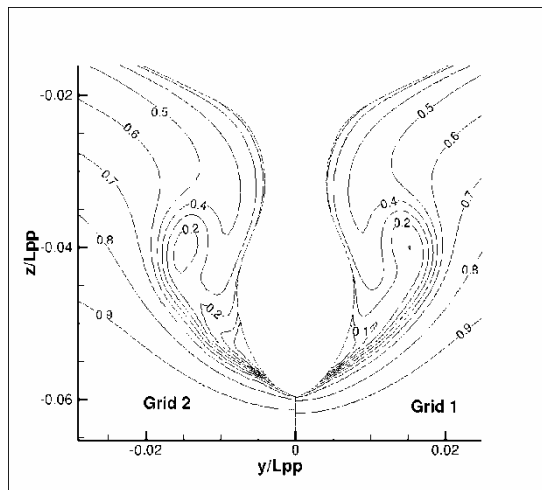


Fig.7: Predicted U velocity contours at section S2

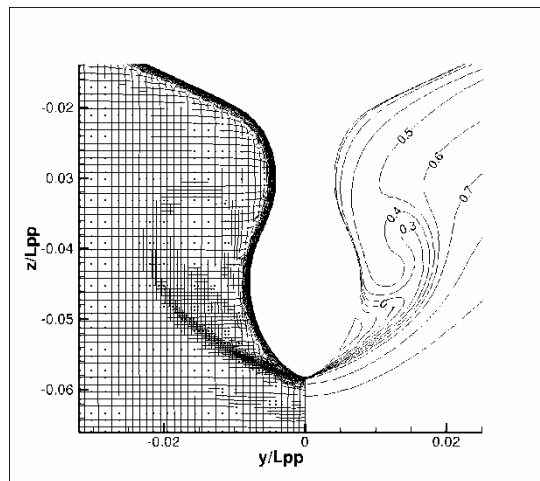


Fig.8: U velocity contours obtained with double model at section S2 with automatic grid refinement

In the core of the aft-body vortex, the predicted axial velocity is higher than measured, while for free-surface computations, the predicted value is lower. This indicates a non-negligible influence of the free-surface deformation on the flow field, despite the low Froude number  $Fn=0.142$ . To clarify this situation, we have performed another adaptive grid refinement computation with free-surface. The minimum cell size was refined to about  $0.00009L_{pp}$ . But with such a fine grid, a flow instability develops leading to an unsteady behavior of the large vortex structure. Due to this unexpected unsteadiness, the predicted wake flow is quite different from what we obtained when the numerical solution converged to a steady solution. Such unsteadiness is also observed when the mesh is refined manually in the wake with similar grid resolution, although in that case, the amplitude of the unsteady fluctuation is not exactly the same. The flow around the naked JBC hull appears therefore to be difficult to be predicted accurately because of a likely unsteady behavior of the main vortex structure.

Additional computations based on hybrid LES turbulence models which are essentially unsteady are currently performed and will be presented at the conference. They will hopefully shed some light on this flow with complex physics.

### 4.3.2 Local flow comparisons with experiments for hull without ESD or propeller

Fig. 9 compares computed and measured longitudinal velocity contours. The computed longitudinal vorticity is slightly weaker than measured. As usually observed, the turbulence anisotropy present in the EASM model contributes to the increase of the longitudinal vorticity (see Fig. 10 which compares at section S2 the isotropic SST and the anisotropic EASM turbulence closures).

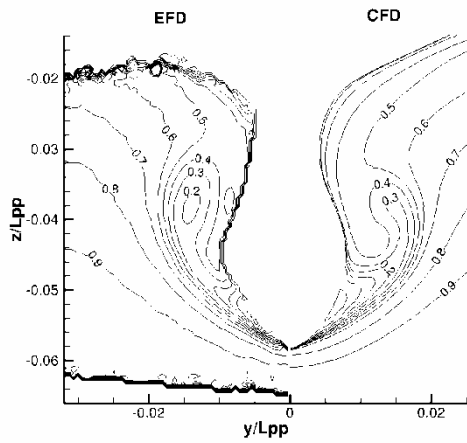


Fig.9: Comparison of U velocity contours at section S2

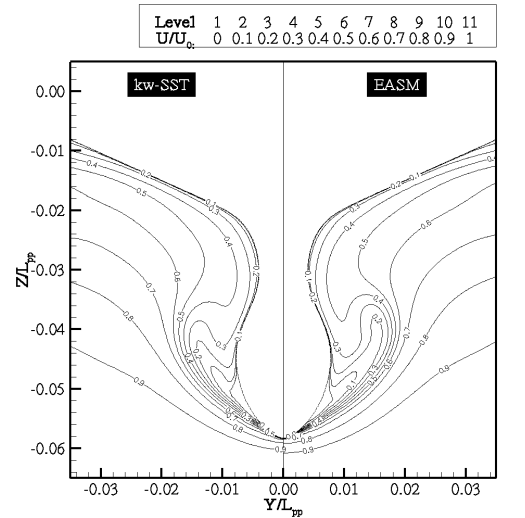


Fig.10: Comparison between SST and EASM model

Figs. 11 and 12 show the wall streamlines on the naked JBC hull without duct or propeller. We can notice a slightly longer line of convergence indicating that the longitudinal bilge vortex is more pronounced with EASM than with SST closures. Moreover, a relatively large zone of recirculation is visible at the stern below the propeller hub, which can be related with the unsteadiness noticed on very fine grids.

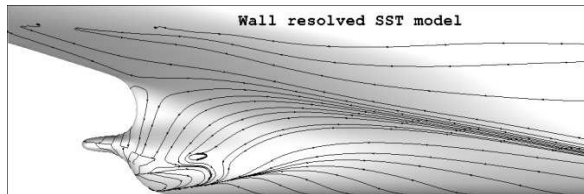


Fig.11: Wall streamlines with SST closure

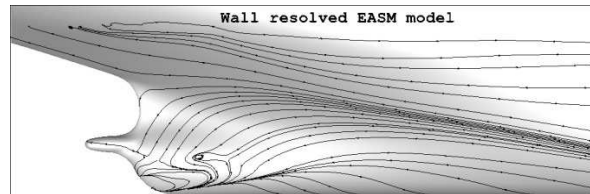


Fig.12: Wall streamlines with EASM closure

### 4.3.3 Local flow comparisons with experiments for hull with ESD and without propeller

Figs. 13 and 14 show the wall streamlines around the hull with the presence of the duct for two different turbulence closures. The main effect of the duct is a suction effect which removes the spiral vortex which was detected by both turbulence closures just above the recirculation region located at the stern of the hull.



Fig.13: Wall streamlines with SST closure

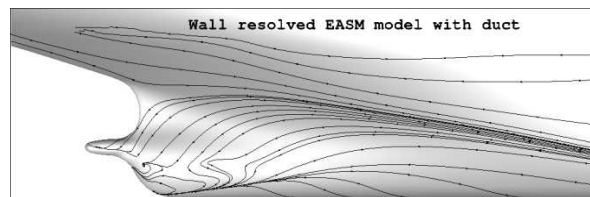
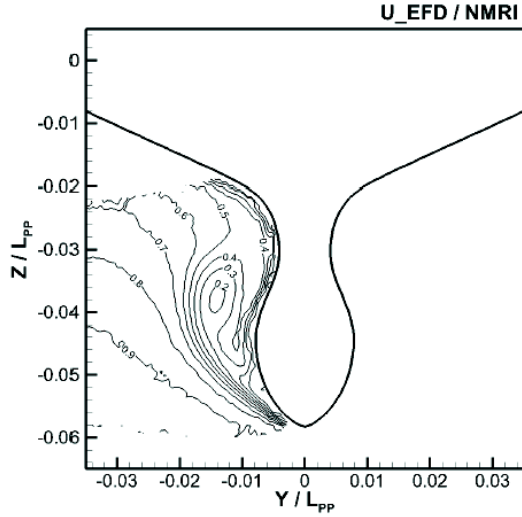


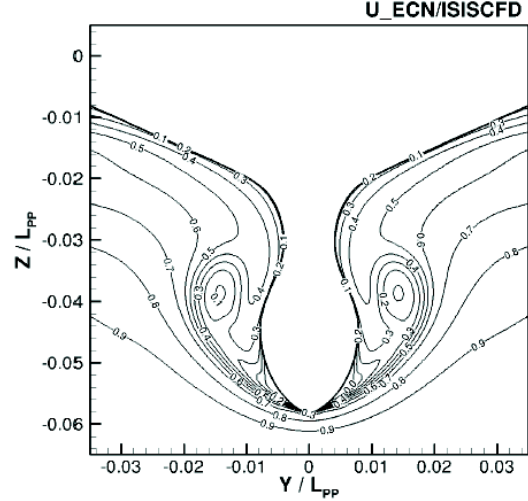
Fig.14: Wall streamlines with EASM closure

Figs. 15 and 16 show the experimental and computed isowake distributions at section S2. We can observe that the presence of the duct increases the computed longitudinal vorticity, leading to an excellent visual agreement between the computations and the measurements at section S2. This agreement is confirmed at section S4 shown in Figs. 17 and 18 although the zone with negative longitudinal velocity seems to be slightly overestimated in the computations.



EFD(NMRI)

Fig.15: Section S2 – Experimental isowake distribution



ECN\_CNRS-ISISCFD-LRN\_EASM

Fig.16: Section S2 – Computed isowake distribution with EASM closure

## 5. Propulsive efficiency improvements due to the ESD

In order to conclude on the influence of the ESD on the ship's propulsion system, self-propulsion parameters are computed for both experiments and simulations and compared between hull configurations (see Figs. 19 and 20 for the duct propeller actual configuration). Two additional modeling approaches for the propulsion system, namely actuator disk (AD) and rotating propeller (RP), used in *del Toro Llorens (2015)*, are compared along this assessment. Apart from the already introduced dimensionless coefficients such as  $J$ ,  $K_T$ ,  $K_Q$  and  $w_t$ , we introduce:

$$t = \frac{T + SFC - R_{T,Towing}}{T}$$

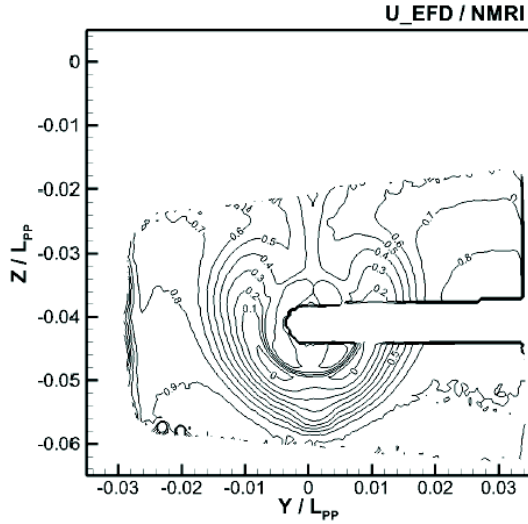
$$\eta_0 = \frac{JK_T}{2\pi K_{Q,OW}}$$

$$\eta_R = \frac{K_{Q,OW}}{K_Q}$$

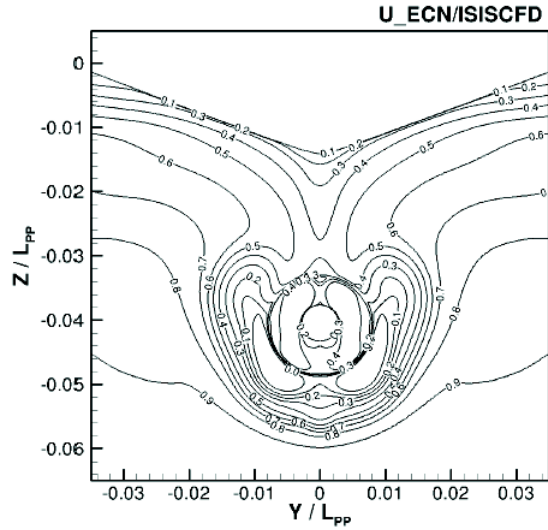
$$\eta_H = \frac{1 - t}{1 - w_t}$$

$$\eta_D = \eta_0 \cdot \eta_R \cdot \eta_H$$

$t$ ,  $\eta_0$ ,  $\eta_R$ ,  $\eta_H$  and  $\eta_D$  are thrust deduction factor, propeller open-water efficiency, relative rotative efficiency, hull efficiency and propeller quasi-propulsive coefficient, respectively. These coefficients are summarized in Tables 7 and 8 which allow comparing the performance of each propulsion modeling approach besides the efficiencies between using or not ESD. The coefficients for both configurations without and with ESD were computed using the simulations with the wall-function modeling approach.



EFD(NMRI)



ECN\_CNRS-ISISCFD-LRN\_EASM

Fig.17: Section S4 – Experimental isowake distribution

Fig.18: Section S4 – Computed isowake distribution with EASM closure

Table 7: Hull without duct and propeller - Summary of propulsive and efficiency coefficients

Parameter	EFD	AD		RP			
		$S_1$	$E\%D$	$S_2$	$E\%D$	$S_3$	$E\%D$
$K_T \times 10$	2.170	2.130	1.84	2.154	0.74	2.144	1.20
$K_Q \times 10^2$	2.790	2.907	-4.19	2.968	-6.38	2.977	-6.70
$K_{Q,OW} \times 10^2$	2.830	2.958	-4.51	2.835	-0.17	2.826	0.15
$n$	7.800	7.620	2.31	7.800	0.00	7.800	0.00
$T$	22.589	20.946	7.27	22.219	1.64	22.113	2.11
$R_{T,Towing}$	36.363	35.668	1.91	35.668	1.91	35.668	1.91
$t$	0.196	0.166	15.26	0.214	-9.13	0.210	-7.21
$w_t$	0.448	0.488	-8.92	0.432	3.60	0.429	4.32
$J$	0.411	0.390	5.06	0.423	-2.93	0.425	-3.51
$\eta_0$	0.5013	0.4470	10.83	0.5113	-2.00	0.5134	-2.42
$\eta_R$	1.0144	1.0175	-0.30	0.9552	5.84	0.9493	6.42
$\eta_H$	1.4575	1.6298	-11.82	1.3845	5.00	1.3833	5.09
$\eta_D$	0.7411	0.7412	-0.02	0.6762	8.77	0.6742	9.03

Table 8: Hull with duct and propeller - Summary of propulsive and efficiency coefficients

Parameter	EFD	AD		RP	
		$S_1$	$E\%D$	$S_2$	$E\%D$
$K_T \times 10$	2.330	2.327	0.13	2.304	1.12
$K_Q \times 10^2$	2.950	3.046	-3.25	3.097	-4.98
$K_{Q,OW} \times 10^2$	2.977	3.101	-4.18	2.871	3.53
$n$	7.500	7.330	2.27	7.500	0.00
$T$	22.435	21.214	5.44	21.966	2.09
$R_{T,Towing}$	36.288	35.752	1.48	35.752	1.48
$t$	0.189	0.168	11.30	0.196	-3.75
$w_t$	0.522	0.558	-7.02	0.502	3.86
$J$	0.370	0.350	5.51	0.386	-4.21
$\eta_0$	0.4615	0.4180	9.42	0.4929	-6.82
$\eta_R$	1.0090	1.0181	-0.90	0.9272	8.11
$\eta_H$	1.6949	1.8837	-11.14	1.6122	4.88
$\eta_D$	0.7892	0.8016	-1.58	0.7368	6.63

Despite the fact that the uncertainty related to the previous results is unknown and for both configurations with and without duct, the self-propulsion point was not achieved, the computations performed modeling the propulsion system with a rotating propeller seem to be slightly more accurate than with actuator disk. The full rotating propeller computation is about ten times more expensive than the actuator disk approach. This is the price to be paid if local flow predictions accounting for the complete hull-ESD-propeller interactions are required. Finally, both measurements and simulations reveal an efficiency gain when the ESD is installed, see Tables 7 and 8; so it is working as expected. However, discrepancies appear between EFD and CFD on how much this gain is. EFD gives a gain in propulsive efficiency of 6.5%, CFD around 8.2% - 9.0% depending on the propulsion modeling approach.

## 6. Conclusions and perspectives

This paper has presented many computations performed on the Japan Bulk Carrier for the last Tokyo 2015 workshop on numerical ship hydrodynamics. A grid influence study was carried out to evaluate the influence of the discretisation error. A preliminary comparison with available experiments was reported for the cases with and without ESD to try to quantify the influence of the duct on the local flow and consequently, on the propulsive efficiency. However, only RANSE computations were performed and the fine grid computations seem to indicate that the flow is not fully steady everywhere. It would be interesting in the future to have recourse to unsteady hybrid LES computations in order to get more physically reliable results and see what the influence of this local unsteadiness on the global flow is. Full-scale computations were not shown due to a lack of time but future studies will be devoted to evaluating the scale effects on the propulsive efficiency associated with the use of this particular Energy Saving Device.

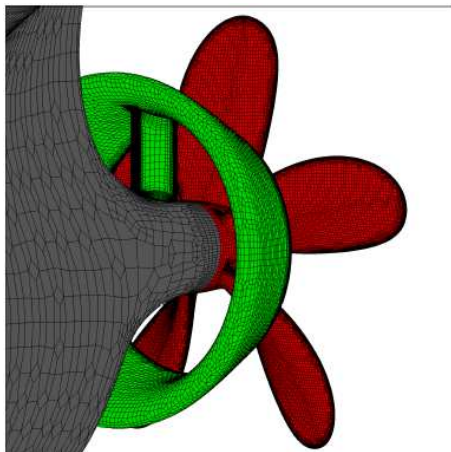


Fig.19: Front view of the propeller + ESD

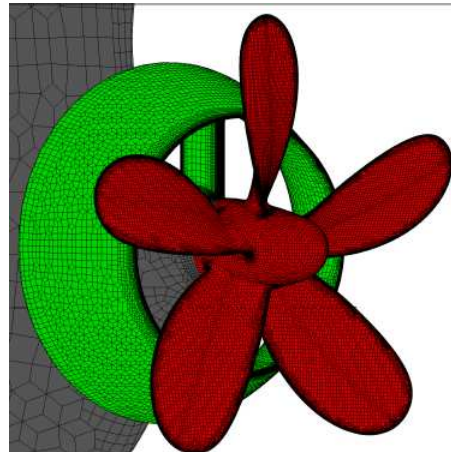


Fig.20: Rear view of the propeller + ESD

## Acknowledgement

This work was granted access to the HPC resources under the allocation 2015-2a1308 made by GENCI (Grand Equipement National de Calcul Intensif).

## References

- DEL TORO LLORENS, A. (2015), *CFD Verification and Validation for Ship Hydrodynamics*, Master Thesis, Ecole Centrale de Nantes
- HOEKSTRA, M.; ECA, L. (2008), *Testing Uncertainty Estimation and Validation Procedures in the Flow Around a Backward Facing Step*, 3rd Workshop on CFD Uncertainty Analysis, Lisbon

QUEUTEY, P.; VISONNEAU, M. (2007), *An Interface Capturing Method for Free-Surface Hydrodynamic Flows*, Computers & Fluids 36/9, pp.1481-1510

WACKERS, J.; DENG, G.B.; LEROYER, A.; QUEUTEY, P.; VISONNEAU, M. (2012), *Adaptive grid refinement algorithm for hydrodynamic flows*, Computers & Fluids.55, pp.85-100